Characterization of Strain-Rate Sensitivity of Sn-5%Sb Solder Using ABI Testing

K. Linga Murty and Fahmy M. Haggag

North Carolina State University
Raleigh, North Carolina 27695-7909

Advanced Technology Corporation
115 Clemson Dr., Oak Ridge, TN 37830

Abstract

A thorough knowledge of the mechanical and fracture properties of solder materials is required both for life-prediction and alloy development. Often only a limited amount of material is available precluding the usage of full-size specimens and thus hardness testing is usually resorted to, which, however, would not give the full stress vs strain characteristics. Whereas, these stress vs strain characteristics can be obtained using the ball indentation. We applied the recently developed Automated Ball Indentation (ABI) tester to evaluate the strain-rate-sensitivity (SRS) of Sn5%Sb solder material at room temperature by varying the indenter velocity over three orders of magnitude. Constant load creep tests were also performed on the same material which covered the low strain-rate range and were in good agreement with ABI. The tensile test results exhibited slight deviation albeit in reasonable agreement with creep and ABI data. While power-law stress dependence is observed at low stresses, results at high ($\geq 1.2 \times 10^{-3} E$) stresses followed an exponential law characterized by an activation area of $\sim 100 b^2$. The underlying deformation micromechanism is discussed.

Introduction

Currently there is an extensive effort in the development of lead-free solders for applications in electronic packaging and Sn5%Sb has been characterized as a credible candidate particularly in multi-chip packages and arrangements where solder materials with varied melting points are needed [10]. While the melting point of this alloy (518K) is high, it has good creep resistance and mechanical strength as well as ductility at ambient. In addition, it has good wettability with 43 ± 4^{o} contact angle. The mechanical properties and creep characteristics have been studied (and also under investigation) in the bulk using the standard tensile and creep specimens [2]. There is a dire requirement to develop techniques to characterize the mechanical, creep, and fatigue properties on the solder structures so that these properties can be gleaned in the *real* situations where the amounts of material available are very small and thus the properties could be different. Moreover, such methodologies will be of great value in monitoring the *in-service* degradation of the mechanical characteristics which will be useful in evaluating life-extension and integrity of such structures [3,4]. Thus these techniques should also be non-destructive and of course cost effective. One such technique is the Automated Ball Indentation (ABI) which has been demonstrated to yield the stress-strain behaviors of many structural metals such as ferritic steels, stainless steels, aluminum alloys

Microstructures and Mechanical Properties of Aging Materials II
Edited by P.K. Liaw, R. Viswanathan,
K.L. Murty, D. Frear, and E.P. Simonen
The Minerals, Metals & Materials Society, 1996

etc. [5,6]. While the idea of ball indentation is not new [8], the uniqueness of ABI lies in the fact that this technique does not require post measurement of the diameter of indentation using elaborate profilometry, optical interferometry, etc., which render the traditional methodology unsuitable for on-line monitoring of the mechanical properties of structures in-service. We apply this ABI technique to characterize the stress-strain characteristics of Sn5%Sb alloy using the recently developed stress-strain microprobe (also know as field indentation microprobe) and obtain the strain-rate sensitivity or the stress exponent at ambient for comparison with the tensile and creep tests on the same material. ABI is a relatively simple, rapid (~ few minutes) and nondestructive technique, requires small amounts of material with essentially no specimen preparation, and can be adopted for *in-situ* testing on *real* structures. Extensions of the methodology can be made for high temperature studies as well as indentation fatigue, fracture [7], and creep.

Experimental Details

Material

Tin-antimony alloy with chemical composition Sn-5%Sb was obtained in the form of 1 mm thick sheet from Alpha Metals, Inc. Flat tensile specimens with a gage length of 1.24 cm were machined from the sheet parallel to the rolling direction for tensile and creep testing. The shoulder portions of these specimens were used for ABI tests so that the specimen to specimen scatter is eliminated or minimized facilitating a direct comparison of the ABI and the standard mechanical tests. No specific specimen preparation is necessary except to make sure that the specimen is flat and the surfaces are parallel. A light mechanical polish was given to remove any surface contamination that might have been accumulated.

ABI Testing

The ball indentation tests were performed on a table top system Model PortaFlow-P1 using a tungsten carbide spherical indenter of diameter, D of 1.575 mm (0.061") with the maximum depth of penetration (h_{max}) of about 0.1 mm (0.004"). A photograph of the system is shown in Fig. 1a, and Fig. 1b depicts close-up of the indenter and LVDT arrangement. The indenter velocity was varied from 5.08×10^{-4} to 0.508 mm/sec (2×10^{-5} to 0.02 in/sec) and the indentation load versus depth were continuously measured using an on-line load cell and an LVDT, respectively (Fig. 1b). At the maximum indentation depth of 0.1 mm, the diameters of indentations were less than 0.375 mm while the specimen thickness is about four times this value. At the same time, because of the relatively small (10 μm) grain size a large number of grains is covered.

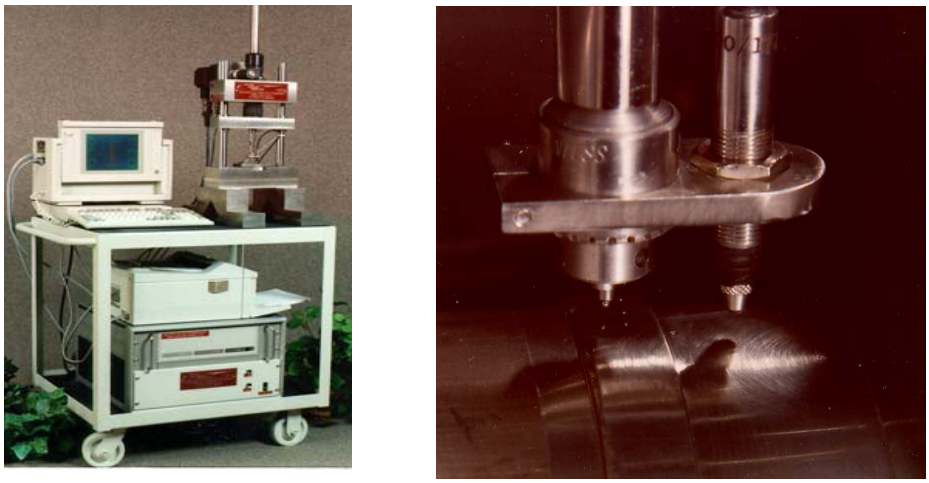

(a) Fig. 1 (b)

Table-Top ABI System Model PortaFlow-P1 (a) and Close-Up (b) of Indenter and LVDT

Typical load versus deformation (depth) curves are included in figures 2a and 2b corresponding to different indenter speeds. A number of tests could be performed in a limited space on the specimen shoulder. All tests were completely computer controlled and the unloading portion at the end of each ABI test was used to determine the system compliance which was evaluated by the computer software.

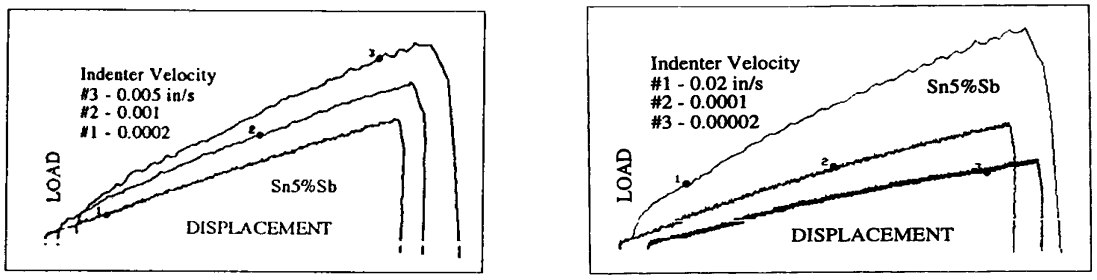

(a) Figure 2 (b)
Indentation Load versus Depth Curves at Varied Indenter Speeds

In addition to the various input parameters, the system software package lists the result for the yield strength, work-hardening parameter, tensile strength as well as Brinell hardness along with many other details. All of these results are printed in both the SI and English units for convenience. A brief summary of the relevant equations used in the derivation of the flow properties is included here while the details may be found in various references [5,6]. As noted in figures 2a and 2b, the primary information obtained from ABI tests comprises the indentation load (P) and the depth/height of penetration (h_p). The system software calculates the plastic strain while the flow stresses are evaluated using elastic and plastic analyses [5]. The true plastic strain is given by [8],

$$\varepsilon_p = 0.2\frac{d_p}{D} \quad , \tag{1}$$

where d_p and D are the *plastic* indentation diameter and diameter of indenter respectively. The corresponding flow stress is calculated using [5,9],

$$\sigma_i = \frac{4P}{\pi d_p^2 \delta} \quad , \tag{2}$$

where σ_i is the true indentation stress, P is indentation load and δ is a parameter which depends on the system compliance and indentation stress with a value between $1.12\alpha_m$ and $2.87\alpha_m$; α_m is a factor which depends on the strain rate sensitivity with a value of unity for strain-rate insensitive materials. The plastic indentation depth, d_p, is given by,

$$d_p = \sqrt[3]{2.735\,P\left(\frac{1}{E_i}+\frac{1}{E_s}\right) D\left\{\frac{h_p^2+0.25d_p^2}{h_p^2+0.25d_p^2-h_pD}\right\}} \quad . \tag{3}$$

Here, E_i and E_s represent the elastic moduli of the indenter and the specimen respectively. As we note here, the parameter d_p appears in both the left and right hand terms and thus an iterative solution is sought which the software of the system has the capability to evaluate. The plastic stress and strain can be related by the power law,

$$\sigma_i = K\,\varepsilon_p^{n'}, \tag{4}$$

where K and n' are the strength coefficient and the strain-hardening parameter respectively. From

the fact that the strain-hardening parameter, n', is equal to the true uniform strain, one can evaluate the tensile stress (σ_{TS}),

$$\sigma_{TS} = K\,(n')^{n'}. \tag{5}$$

The ultimate tensile strength (nominal value) is then obtained from

$$UTS = K\{\frac{n'}{e}\}^{n'} . \tag{6}$$

In addition to the UTS, one often requires the yield strength which can also be obtained from the flow rule. However, it is found to be convenient to relate the indentation load and diameter through Meyer's coefficient (m'),

$$\frac{P}{d_i^2} = A'\{\frac{d_i}{D}\}^{m'-2} . \tag{7}$$

The constant A' is a material parameter through which one may find the yield strength (σ_y),

$$\sigma_y = B_m A'. \tag{8}$$

In this equation, B_m is a material constant and has a value of 0.2285 for carbon steels. Extensive correlations by Haggag et al [5-7] revealed good correlation between ABI and tensile data for many ferritic steels with essentially identical B_m value. Another factor that is derived from the ABI data and is a part of the system software is the Brinell hardness (HB) obtained from,

$$HB = \frac{2}{\pi D}\frac{P_{max}}{D - \sqrt{D^2 - d_{max}^2}} . \tag{9}$$

It is clear from the above description that many useful mechanical property data can be obtained from ABI and extensive correlations have been made for many structural metals.

Results and Discussion

Figures 2a and 2b depict the indentation load versus depth of penetration curves for Sn5%Sb obtained at varied indenter speeds corresponding to different strain-rates. The strain-rate is evaluated from the indenter speed [9],

$$\dot{\varepsilon} \approx \frac{2}{5}\frac{v_i}{d_p} , \tag{10}$$

where v_i is the indenter velocity and d_p is the plastic indenter diameter at the point of interest. Table 1 summarizes the results and both the flow stress at 0.067 plastic strain and tensile stress are included. As expected, the stress increased with the increasing strain-rate. The effect of flow stress on the strain-rate is shown on a double log plot in Figure 3 which reveals that the data set breaks into two distinct regions.

At low stresses, the strain-rate followed a power-law equation such as is commonly noted in high temperature deformation,

$$\dot{\varepsilon} = A\,\sigma^n = A_L\,\sigma^{4.5} , \tag{11a}$$

where n is the stress exponent which is the inverse of the strain-rate-sensitivity (m),

$$\sigma = A'\,\dot{\varepsilon}^{\,m} , \; m = 0.222. \tag{11b}$$

At high stresses, strain-rates increase much faster and the data may be fit to a similar equation with n=8.6 (or m=0.116). However, an exponential stress dependence is more relevant as is shown below. We now compare the ABI data with creep and tensile results.

Table 1
Room Temperature ABI Results - Sn-5%Sb

Speci-men #	Indenter Velocity in/s	Strain-Rate per sec	Flow Stress* Mpa	σ_{TS} Mpa
7	$2x10^{-5}$	$2.930x10^{-4}$	13.1	31.1
8	$5x10^{-5}$	$7.326x10^{-4}$	16.5	39.3
6	$1x10^{-4}$	$1.465x10^{-3}$	18.6	44.1
1	$2x10^{-4}$	$2.930x10^{-3}$	18.6	49.6
2	$2x10^{-4}$	$2.930x10^{-3}$	20.6	46.8
3	$1x10^{-3}$	$1.465x10^{-2}$	23.4	56.5
4	$5x10^{-3}$	$7.326x10^{-2}$	28.9	65.5
5	$1x10^{-2}$	$1.465x10^{-1}$	29.6	69.6

*at $\dot{\varepsilon}_p \approx 0.067$

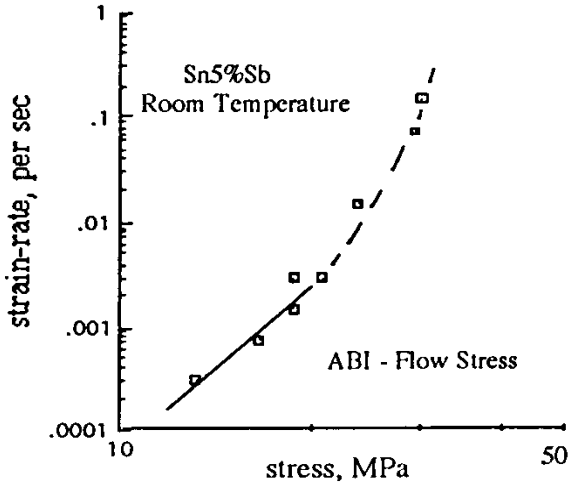

Figure 3
Double-Log Plot of Strain-Rate versus Stress

As described in more detail by Mahidhara et al [2], creep tests were performed on Sn5%Sb using a dead-load creep machine on the same specimens on which ABI tests were made. Figure 4 includes the creep data plotted as the steady-state creep-rate versus applied stress, and we note that the creep results fall below the ABI data, albeit they are parallel, both yielding values of 4.5 for the stress exponent. The ABI data span relatively large stress and strain-rate range towards higher levels. Mechanical properties derived from tensile tests at various temperatures and at room temperature are also included for comparison. We note that these data also fall below the ABI results although the creep and tensile data are in closer agreement to each other.

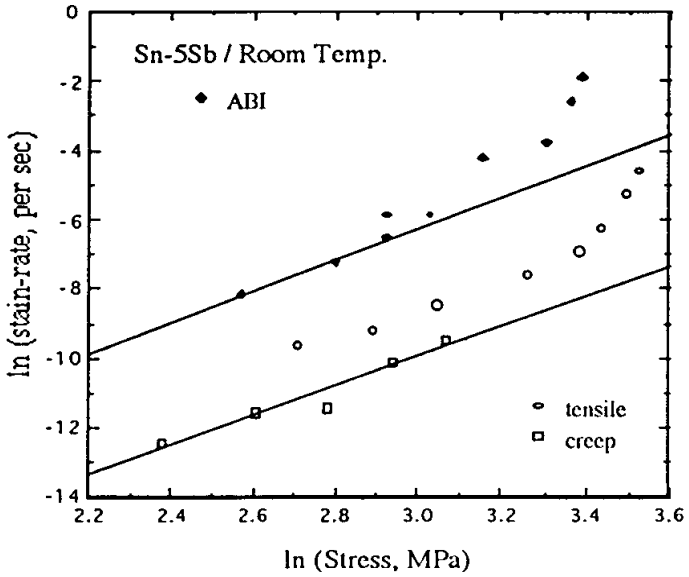

Figure 4 Comparison of ABI (Flow Stress) with Tensile and Creep Results

It should be pointed out that the tensile test results correspond to the ultimate tensile stresses and a correlation with creep is expected only when ultimate tensile stresses are used. Thus in Figure 5 we compare the ABI results in terms of both the flow and tensile stresses with those of creep, the slopes of the curves yielding the strain-rate sensitivity, as is commonly done in the analyses of constant strain-rate and strain-rate change tests [1,2]. We note a close agreement between the creep and ABI data with ultimate tensile stresses in place of the flow stress. Although there is no overlap of these two data sets, high stress creep data extrapolate to the low stress ABI results prior to the onset of the very high stress regime corresponding to exponential stress dependence of the strain-rate.

The excellent correlation between creep and ABI (tensile stress) results and the deviation of the tensile test data from these two sets indicate possible specimen-to-specimen differences since the same specimens are used for creep and ABI tests. Since all the samples were taken form the same lot of material, these material differences cannot be a major factor. It is possible that relatively large strains accumulated prior to reaching maximum load in the tensile tests have an effect on the calculation of the true stress and true strain-rate. More significantly, often the load maximum is not a point but occurs over a relatively large displacement or strain thereby leading to deviations from the exact tensile strength evaluation.

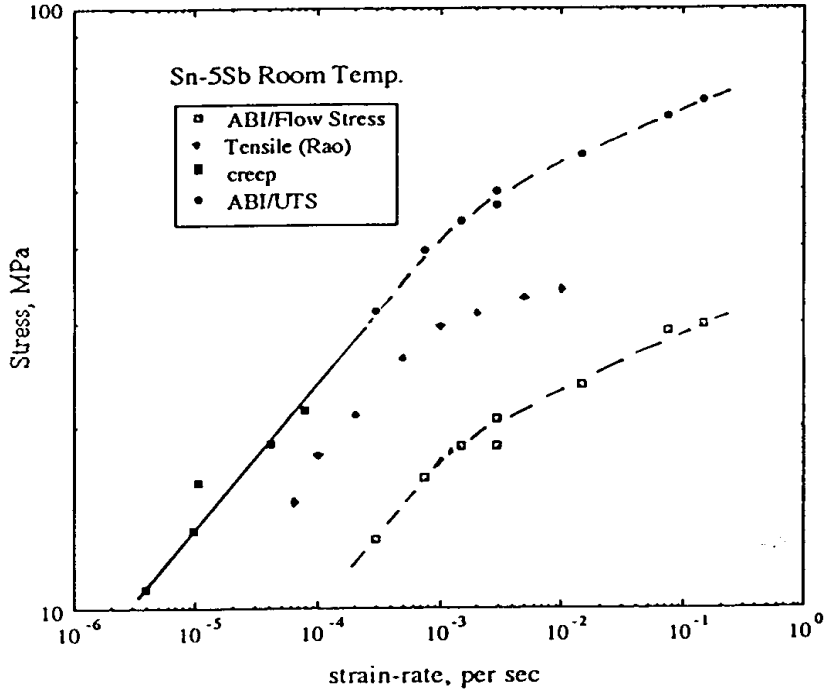

Figure 5
Log-Log Plot of Stress versus Strain-Rate-
Comparison of Tensile and Creep Results with ABI

Deformation Mechanism

As is clear from the above description, the appropriate correlation is achieved in using ABI data with ultimate tensile stresses, and Figures 6a and 6b depict the effect of tensile stress on the strain-rate in low and high stress regimes respectively. The low stress range is analyzed in terms of a power-law while the high stress data are correlated using an exponential stress dependence. Thus the low stress regime is shown on a double-log plot (Fig. 6a) while data in the high stress region are depicted in a semi-log plot (Fig. 6b). Such dependencies are expected for Sn5%Sb at ambient because of its low melting point, room temperature corresponds to relatively high homologous temperature ($\geq 0.5T_M$) where dislocation creep mechanisms become dominant.

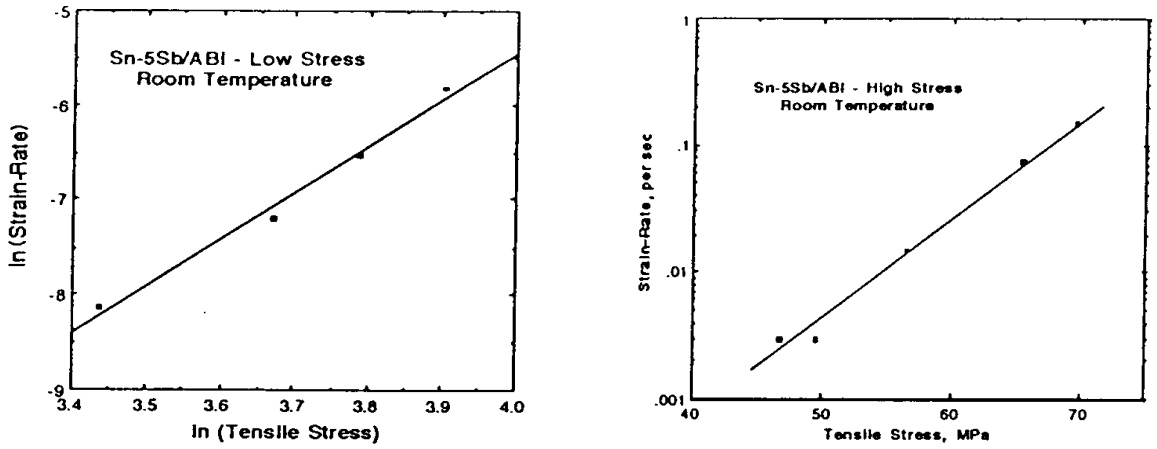

Figure 6
Stress Dependence of Strain-Rate in the Low (a) and High (b) Stress Regions

The slope of the line in Fig. 6a has a value of 4.5 (stress exponent) which indicates deformation controlled by the dislocation mechanisms such as the climb of edge dislocations and motion of jogged screw dislocations [10]. At stress equal to or higher than ~$1.23\text{x}10^{-3}$ E, we find an exponential variation of the strain-rate (Fig. 6b),

$$\dot{\varepsilon} = A_L \, \sigma^{4.5} \quad \text{(low stresses, Fig. 6a),} \tag{12a}$$

and

$$\dot{\varepsilon} = A_H \, e^{B'\sigma} \quad \text{(high stresses, Fig. 6b).} \tag{12b}$$

Here, B' = 0.182 with σ in Mpa. The critical stress for the transition from power-law creep to exponential stress region is commonly referred to as the power-law breakdown, and the present value of $1.23\text{x}10^{-3}$E is in close agreement with creep data on many pure metals and alloys [10, 11]. The exponential dependence of the strain-rate on the stress implies that the deformation mechanism is characterized by a stress-independent activation area, A*, given by,

$$A^* = \frac{2kT}{b}\left\{\frac{d\ln\dot{\varepsilon}}{d\sigma}\right\}_T \quad , \tag{13}$$

where b is the Burger's vector. Physically, the activation area may be interpreted as the area swept out by a dislocation segment in surmounting a barrier in its slip plane or the area swept out between consecutive events. ABI data in Fig. 6b yield a value of $96.5b^2$ and values of ~$10b^2$ to $100b^2$ correspond to the climb of the edge dislocations as the dominant mechanism versus nonconservative glide of jogged screw dislocation with a characteristic activation areas in excess of $1000b^2$ [12]. One may combine the two equations (12a and 12b) using a Sinh-function so that the whole data set may be described by a single equation,

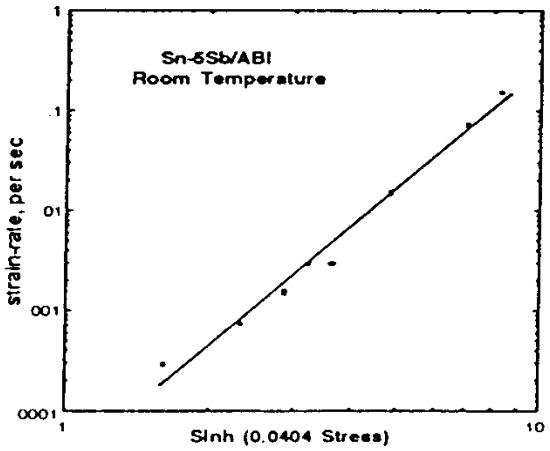

Figure 7

Double Log Plot of Strain-Rate
versus Sinh (Bσ)

$$\dot{\varepsilon} = A\,(\text{Sinh } B\sigma)^n = 1.235\text{x}10^{-5}\,(\text{Sinh } 0.04\sigma)^{4.5}. \quad (14)$$

Here, $\dot{\varepsilon}$ is in per sec and σ is in Mpa. This implies that a double plot of strain-rate versus Sinh $B\sigma$ should yield a straight line as indicated in Figure 7 with the slope of the line being 4.5.

Conclusions

ABI is a relatively simple technique to characterize mechanical properties of materials in particular solders. Room temperature ABI data on Sn5%Sb correlated well with both tensile and creep results. Dislocation micromechanisms can be investigated using ABI tests at varied strain-rates. Compared to conventional tests, ABI technique has many advantages: small amounts of material are adequate, no extensive specimen preparation is necessary, extensions to *in-situ* tests on *real* structures can be made and thus the method is useful in monitoring in-service mechanical property changes. Further work is warranted for extension to high temperatures as well as for indentation fatigue, fracture and creep testing using ABI technique.

References

1. R. K. Mahidhara, S. M. L. Sastry, I. W. Turlik and K. L. Murty, *Scripta Met.* vol. 31, No. 9 (1994) 1145.
2. R. K. Mahidhara, P. Markle, K. L. Murty and I. Turlik, "Tensile and Creep Behavior Sn-5%Sb Solder," this proceedings.
3. K. L. Murty, H. Yang and I. Turlik, "Application of Deformation Mechanism Maps to Solder Reliability in Electronic Packaging," Proceedings NEPCON West 1993.
4. R. Darveaux, K. L. Murty and I. Turlik, "Predictive Thermal and Mechanical Modeling Applied to the MCNC Multichip Module," *Journal of Metals,* July (1992) 36.
5. F. M. Haggag, "In-Situ Measurements of Mechanical Properties Using Novel Automated Ball Indentation System," *Small Specimen Test Techniques Applied to Nuclear Reactor Vessel Thermal Annealing and Plant Life Extension,* ASTM STP 1204, W.R. Corwin, F. M. Haggag and W. L. Server, eds., American Society for Testing and Materials, Philadelphia, (1993) 27.
6. F. M. Haggag and G. E. C. Bell, "Measurement of Yield Strength and Flow Properties in Spot Welds and Their HAZs at Various Strain-Rates, *International Trends in Welding Science and Technology,* S. A. David and J. M. Vitek, eds., ASM, Materials Park, OH (1993) 637.
7. F. M. Haggag and R. K. Nanstad, "Estimating Fracture Toughness Using Tension or Ball Indentation Tests and a Modified Critical Strain Model," *Innovative Approaches to Irradiation Damage and Failure Analysis,* D. L. Marriott et al, eds., Pressure Vessel and Piping, vol. 170, ASME (1989) 41.
8. D. Tabor, *The Hardness of Metals,* Oxford University Press, New York (1951).
9. H. Francis, "Phenomenological Analysis of Plastic Spherical Indentation," Trans. ASME, July (1976) pp. 272-281.
10. K. L. Murty, F. A. Mohamed and J. E. Dorn, *Acta Metall.*, vol. 20 (1972) 1009.
11. O. D. Sherby and P. M. Burke, *Prog. in Mat. Sci.*, vol. 13 (1967) 325.
12. K. L. Murty, M. Gold and A. L. Ruoff, *Journal of Applied Physics*, vol. 41 (1970) 4917.